JOINT EUROPEAN TORUS JET

JET–P(87)30

R. Giannella, V. Zanza, E. Barbato, G. Bracco, S. Corti
and D.J. Gambier

Neutral Particle Emission in JET during Radio Frequency Heating Experiments

Neutral Particle Emission in JET during Radio Frequency Heating Experiments

R. Giannella[1], V. Zanza[1], E. Barbato[1], G. Bracco[1], S. Corti and D.J. Gambier[2]

JET-Joint Undertaking, Culham Science Centre, OX14 3DB, Abingdon, UK

[1]Centra Ricerche Energia Frascati, Associazione Euratom-ENEA sulla Fusione, Frascati, Rome, Italy.
[2]Centre d'études nucléaires de Cadarache, Association Euratom-CEA sur la fusion, Saint-Paul-lez-Durance, France.

Preprint of Paper to be submitted for publication in Nuclear Fusion

NEUTRAL PARTICLE EMISSION DURING ICRF HEATING EXPERIMENT IN JET

R Giannella*, V Zanza*, E Barbato*,
G Bracco*, S Corti, D J Gambier°

JET Joint Undertaking, Abingdon, Oxon, OX14 3EA, UK

* EURATOM-ENEA Association, Frascati, Italy
° EURATOM-CEA Association, Cadarache, France

Abstract

In this paper we deal with the simulation of neutral particle spectra obtained in JET with an array of four passive neutral particle analysers during discharges where stationary or modulated RF power is applied in the Ion Cyclotron Range of Frequencies for a deuterium plasma with hydrogen minority.

To compute the distribution function of the hydrogen ions a one dimensional Fokker-Planck equation has been used where the wave particles interaction is described by a quasi-linear diffusion term in the velocity space. Both stationary and oscillating solutions of the Fokker-Planck equation have been worked out and the computed hydrogen fluxes are found to be in very good agreement with the measured ones. In this context the problems arising in the deduction of the power deposition profiles in modulated discharges are discussed.

As a result, the profiles of power delivered to the electrons and to the bulk ions have been obtained. It is further shown that no adjustable parameters need to be introduced and that the main source of error lies in the uncertainty in the knowledge of the ion density.

1. INTRODUCTION

In minority plasma heating experiments performed with waves in the Ion Cyclotron Range of Frequencies (ICRF) a major role is usually played by the high energy ion tails /1,2,3/. In fact the mechanism of resonant absorbtion of the wave leads to the production of suprathermal ions that, in turn, deliver their energy to the bulk ions and electrons via Coulomb collisions.

The study of these tails, is in general rather complicated because it is not possible to separate the problem of generation and thermalization of the suprathermal populations from the one of their transport across the plasma.

In this respect the JET tokamak is particularly well adapted for this kind of studies. In fact, due to the large ratio between the scale length of the plasma cross section and the ions gyro-radius and due to the very small magnetic field ripple, the importance of the transport of the energetic ions is largely reduced. As a consequence the energy deposition profile can be better assessed, and the theoretical model describing the absorption of the waves can be accurately cross checked with the experimental results from space and mass resolved measurements of neutral particle fluxes in a range of energies much wider than the thermal one.

In this paper an analysis is presented of the charge-exchange neutral hydrogen and deuterium measurements performed on some ICRF heated JET discharges.

In section 2 a brief description of the experimental conditions is given. Section 3 deals with the solution of the Fokker-Planck equation for both stationary and modulated cases, while in sections 4 and 5 we present the results of the simulation of the experimental data for stationary and modulated discharges respectively. Finally, in section 6, these results are summarized and discussed.

2. EXPERIMENTAL CONDITIONS AND DATA ANALYSIS

The JET tokamak and its experimental operation have been thoroughly described in the literature /4,5/. In particular additional heating using waves in the ion cyclotron range of frequencies has successfully been applied with three antennas energized in different electrical configurations at power levels higher than the highest ohmic power /6,7/. In some cases the ICRF power has been modulated, mainly with the aim of determining the power deposition profile /8/ and of getting information about the transport of thermal energy /9/.

In this paper we focus on the case of hydrogen minority heating in which the RF frequency has been chosen so that the hydrogen minority resonance in the deuterium plasma ($n_H/n_D \lesssim 0.05$) is located at a radius close to the magnetic axis. The range of plasma parameters are typically:

- peak electron density n_e=2 - 3.5x10^{19} m^{-3},
- electron temperature T_e=3 - 5 keV,
- ion temperature T_i=2.5 - 4 keV,
- magnetic field B_T= 2.1 - 3.2T,
- plasma current Ip= 2 - 3 MA,
- average ICRF coupled power P_{RF}=0.6 - 5 MW
- Z_{eff}~3.

The neutral particle fluxes are measured by a system of four identical analysers looking at different chords whose minimum distance from the plasma centre ranges from 0 to about 60cm. All the lines of sight are in the same vertical plane whose angle with respect to the magnetic axis was fixed to ≈ 105°. The analysers, fully described in ref./10/ together with the calibration procedures and results, measure simultaneously the spectra of both hydrogen and deuterium over a wide range of energies. Deuterium fluxes were detected in the energy range 3-45 keV and hydrogen ones in the range 6-90 keV. For

the purpose of studying the minority tails it would have been interesting to have measurements at energies much higher than the ones actually scanned, but, due to the steep decrease of the charge exchange cross-section with energy, the signal to noise ratio would have been too low.

In fig. 1 the measured neutral hydrogen fluxes at 40 keV, are displayed together with the trace of the total coupled power for a discharge where the power of the antennas was modulated. A marked increase of the average flux level is observed only by the analysers looking at the region near the plasma centre, showing that the interaction of the H minority with the RF wave is localized. On these signals, superimposed to the large amplitude oscillations due to the sawtooth activity, an oscillating response to the modulated RF pulse can also be observed.

To analyse quantitatively these data we performed the spectral analysis of the signals making use of the discrete Fourier transform /11/. This well known technique consists essentially in finding, for a signal sequence S_n sampled at times $t_n=t_o + n\Delta t$ $(n=0, 1,..., 2N-1)$, the spectral representation

$$S_n = \frac{1}{\sqrt{2N}} \sum_{k=0}^{2N-1} \hat{S}_k \exp\left[-i \frac{\pi k n}{N}\right] \qquad (1)$$

$$\hat{S}_k^* = \hat{S}_{N-k}$$

Each coefficient $\hat{S}_k$ corresponds to the frequency $\nu_k = \frac{k}{2N\ \Delta t}$ $(k=0, 1,..., N-1)$

In fig. 2 the autocorrelation spectra of the power signal, $/\hat{P}_k/^2$, and of the neutral flux signal at R=0, $/\hat{F}_k/^2$, are shown.

As can be seen the frequency bandwidth of the power signal is narrower than the frequency resolution so that only one coefficient $\hat{P}_{k_m}$ in the spectrum is significant at every harmonic order m. Accordingly the amplitudes of the oscillating responses is deduced from the corresponding coefficients in the spectrum of the flux $a_m = 2/\hat{F}_{k_m}/$. The phases of the corresponding terms in the cross correlation spectrum, $\hat{P}_{k_m} * \hat{F}_{k_m}$ give the relative phase of the two signals.

3. FOKKER-PLANCK EQUATION

Let us write the Fokker-Planck equation describing the evolution of the resonant ion distribution function, $g(\vec{v})$, in the form /12/:

$$\frac{\partial g}{\partial t} = C'(g) + Q'(g)$$

where C'(g) is the collision term and Q'(g) is the quasi-linear RF diffusion term. For the first harmonic interaction scheme Q'(g), in terms of particle velocity, v, and cosine of pitch angle, $\mu = v_{//}/v$, can be written as /13/

$$\begin{aligned} Q'(g) = K \frac{1}{v^2}\Big\{ & (1-\mu^2)\,\frac{\partial}{\partial v}\Big[v^2 \Big| J_o\Big(\frac{k_\perp v_\perp}{\omega_{ci}}\Big)\Big|^2 \frac{\partial g}{\partial v} + \\ & + \frac{\partial}{\partial \mu}\Big[\mu(1-\mu^2)\Big| J_o\Big(\frac{k_\perp v_\perp}{\omega_{ci}}\Big)\Big|^2 \frac{\partial}{\partial \mu}(\mu g)\Big] + \\ & + \frac{\partial}{\partial \mu}\Big[\mu(1-\mu^2)\Big| J_o\Big(\frac{k_\perp v_\perp}{\omega_{ci}}\Big)\Big|^2 \frac{\partial}{\partial v}(vg)\Big] - \\ & - \frac{\partial}{\partial v}\Big[(1-\mu^2)\, v\Big| J_o\Big(\frac{k_\perp v_\perp}{\omega_{ci}}\Big)\Big|^2 \mu \frac{\partial g}{\partial \mu}\Big]\Big\} \end{aligned} \qquad (2)$$

where K is a constant depending on the RF electric field strength; $k_{//}$ and $k_\perp$ are the parallel and perpendicular component of the wave vector respectively and J_o is the zero-order Bessel function of the first kind.

Following the usual procedure $g(v,\mu)$ can be expanded in Legendre polynomials, $g(v,\mu) = f(v) + B(v)\cdot P_2(\mu) + \ldots$

Substituting this last expression in eq.(2) and averaging over μ, we derive the following equation for the isotropic part of the quasi linear term:

$$Q(f) = \frac{1}{v^2}\frac{\partial}{\partial v}\Big[v^2 H \frac{\partial f}{\partial v}\Big] + D(B) + \ldots \qquad (3)$$

where

$$H(v) = K \frac{3}{4} \int_{-1}^{1} (1-\mu^2) \left| J_o\left(\frac{k_\perp v\sqrt{1-\mu^2}}{\omega_{ci}}\right) \right|^2 d\mu \qquad (4)$$

$$H(0) = K$$

$D(B)+ \ldots.$ represent the contribution of the anisotropic part of the distribution function to the quasi-linear term. In the following this term will be neglected. The error introduced in doing so has been estimated by Stix /12/as:

$$\frac{B(v)}{f(v)} \simeq \frac{W}{\frac{3v^2mn}{2\tau_\perp} + \frac{10}{7} W} \qquad (5)$$

where W is the absorbed power density, m and n are the mass and density of resonant ions and $\tau_\perp$ is the pitch angle scattering time.

For the typical plasma parameters considered in this paper: $W \sim 0.1\text{-}0.2$ W/cm^3, $n_e \sim 2\text{-}3.5 \times 10^{13}$ cm^{-3}, $n/n_e \sim 0.03$, the ratio B/f is of the order of 10% or less in the whole energy range. However, in discharges heated with a much higher power the anisotropy of the distribution function must be taken into account, thus requiring a solution of a 2-D Fokker-Planck equation. This is not addressed in the present article because the correction that would result from this effect is smaller than the uncertainties due to the inaccuracies of some experimental data (eg the ion density as pointed out in Section 4).

In the expression H(v) of the quasi-linear diffusion coefficient, the finite Larmor radius effect, is retained through the argument of the Bessel function J_o. This is of some importance in JET since high energy particles are confined. For this class of particles the Larmor radius is a non-negligible fraction of the ICRF wavelength and can lead to a saturation in the absorption process. However, in the experiments reported here, the ICRF power density is moderate

and the fraction of resonant particles reaching $k_\perp v_\perp / \omega_{ci} \geq 1$ is quite small.

Furthermore, the heating scenario in these experiments corresponds to a strong absorption and consequently the problem of the inhomogenity of the RF field /14/ can safely be neglected. For these reasons we used the $k_\perp$ value deduced from the cold plasma dispersion relation with $k_{//}=0$, since the antenna powered was in a monopole configuration where the maximum launched power peaks at $k_{//}=0$.

The Coulomb collision term C(f) for a minority colliding with maxwellian background can be written /15,16/:

$$C(f) = \frac{1}{v^2} \frac{\partial}{\partial v} \left[v^2 \, D \, \frac{\partial f}{\partial v} + v^2 \, F \, f \right] \qquad (6)$$

where the pitch angle scattering term has disappeared due to the average over μ.

In eq.(6) D(v) is the collisional diffusion coefficient and F(v) is the dynamical friction coefficient given by:

$$D = \sum_\beta \frac{\nu_{//}^\beta}{2} v^2 \qquad F = \sum_\beta \frac{m}{m+m_\beta} \nu_s^\beta \, v; \qquad (7)$$

the summation being performed over all the plasma components. The summation over the ion species contains, both for F and D, the common factor $\sum \frac{n_\alpha Z_\alpha^2}{A_\alpha}$ where n_α, Z_α and A_α are the density, charge and mass of the ion of species α. This term, for low hydrogen concentrations, is practically equal to $n_e/2$ and independent of Z_{eff}.

A Z_{eff} dependence is still present in the pitch angle diffusion term which in this case has been averaged out but should be considered to determine the degree of anisotropicity of the distribution function.

Then the Fokker-Planck equation we consider reduces to:

$$\frac{\partial f}{\partial t} = \frac{1}{v^2}\frac{\partial}{\partial v}\left[v^2 D \frac{\partial f}{\partial v} + v^2 F f\right] + \frac{1}{v^2}\frac{\partial}{\partial v}\left[v^2 H \frac{\partial f}{\partial v}\right] \quad (8)$$

Since we will study discharges heated both with a constant and a modulated power, both the steady state and the oscillating solutions of eq.(8) are required.

In order to get such solutions we expand H and f in Fourier components:

$$\begin{aligned} H &= \sum_{-\infty}^{+\infty} H_m e^{-im\omega t} \\ f &= \sum_{-\infty}^{+\infty} f_m e^{-im\omega t} \end{aligned} \quad (9)$$

where $f_m = f^*_{-m}$ are complex numbers. In this paper only sinusoidal or square waves RF power are considered so that H_m can be taken real. In the first case $H_m=0$ for all $m\neq 1$ and -1 while in the second case $H_m=0$ for all even $m\neq 0$.

Substituting into eq.(8) we get

$$\begin{aligned} \sum_m -im\omega f_m e^{-im\omega t} = \frac{1}{v^2}\frac{\partial}{\partial v}\Big[v^2 D \sum_m \frac{\partial f_m}{\partial v} e^{-im\omega t} + \\ + v^2 F \sum_m f_m e^{-im\omega t}\Big] + \\ + \frac{1}{v^2}\frac{\partial}{\partial v}\Big[v^2 \sum_n H_n e^{-in\omega t} \sum_m \frac{\partial f_m}{\partial v} e^{-im\omega t}\Big] \end{aligned} \quad (10)$$

that, after simple manipulation, becomes

$$\begin{aligned} -im\omega f_m = \frac{1}{v^2}\frac{\partial}{\partial v}\left[v^2 (D+H_o)\frac{\partial f_m}{\partial v} + v^2 F f_m\right] + \\ + \frac{1}{v^2}\frac{\partial}{\partial v} v^2 \sum_{n\neq m} H_{m-n}\frac{\partial f_n}{\partial v} \end{aligned} \quad (11)$$

Two coupled equations for f_o and f_1 are then obtained by putting m=0 and m=1 and neglecting terms of the order of $H_{-1}\frac{\partial f_2}{\partial v}$ and higher:

$$\frac{\partial f_o}{\partial v} = -\frac{F}{D+H_o} f_o - \frac{2H_1}{D+H_o} \frac{\partial f_{1R}}{\partial v} \tag{12}$$

$$\frac{\partial}{\partial v}\left[v^2 (D+H_o) \frac{\partial f_1}{\partial v} + v^2 F f_1 + v^2 H_1 \frac{\partial f_o}{\partial v}\right] = -i v^2 \omega f_1 \tag{13}$$

where f_{1R} is the real part of f_1.

For a constant power level, $H_1=0$, eq.(12) can be integrated at once, giving the well known Stix distribution function

$$f_o(v) = A \exp\left\{ - \int_o^v \frac{F\, dv'}{D+H_o} \right\} \tag{14}$$

In order to write the system of equations (12) and (13) in a form suitable for numerical integration we introduce:

$$\phi = v^2 (D+H_o) \frac{\partial f_1}{\partial v} + v^2 F f_1 + v^2 H_1 \frac{\partial f_o}{\partial v} \tag{15}$$

Now, defining ϕ_R as the real part of ϕ, from eqs. (12) and (15) we obtain

$$\frac{\partial f_o}{\partial v} = - \frac{F(D+H_o)}{(D+H_o)^2-2H_1^2} f_o + \frac{2H_1 F}{(D+H_o)^2-2H_1^2} f_{1R} - \frac{2H_1}{v^2[(D+H_o)^2-2H_1^2]} \phi_R \tag{16}$$

and

$$\frac{\partial f_{1R}}{\partial v} = \frac{H_1 F}{(D+H_o)^2-2H_1^2} f_o - \frac{F(D+H_o)}{(D+H_o)^2-2H_1^2} f_{1R} + \frac{(D+H_o}{v^2[(D+H_o)^2-2H_1^2]} \phi_R \tag{17}$$

while, defining f_{1I} and ϕ_I as the imaginary part of f_1 and ϕ respectively, from eq. (15) we get

$$\frac{\partial f_{1I}}{\partial v} = - \frac{F}{D+H_o} f_{1I} + \frac{1}{v^2(D+H_o)} \phi_I \tag{18}$$

and from eq.(13) we get

$$\frac{\partial \phi_R}{\partial v} = v^2 \omega f_{1I} \tag{19}$$

$$\frac{\partial \phi_I}{\partial v} = - v^2 \omega f_{1R} \tag{20}$$

Equations (16) to (20) form a system of five first order coupled equations which can be solved if five boundary conditions are supplied.

The first of these conditions is $f_o(0)=C$, where C must be chosen in order to fulfill the normalization condition.

The remaining four conditions are deduced from particle conservation $\int_0^\infty 4\pi v^2 f_1(v)\, dv = 0$ with the further physical constraint $\phi(0)=0$.

Integrating both sides of eqs.(19) and (20) we obtain

$$\phi_R(0) = \phi_R(\infty) = 0 \tag{21}$$

and

$$\phi_I(0) = \phi_I(\infty) = 0 \tag{22}$$

The system of eqs.(16) to (20) can now be solved. This has been done using the NAG Library routine D02GBF /17/.

Once the components of the distribution function are known, the absorbed power can be computed by:

$$P_{abs} = \int \tfrac{1}{2} m v^2 Q(f) 4\pi v^2 dv \qquad (23)$$

In a similar way also the power going from the minority to the electrons and to the background ions can be calculated.

Inside the square brackets of eq.(13) the term $H_{-1}\frac{\partial f_2}{\partial v}$ has been neglected. This is justified if

$$H_1 \frac{\partial f_{2(R,I)}}{\partial v} << \Phi_{R,I} \qquad (24)$$

This last condition cannot be fulfilled for very low frequencies, as can be seen from eqs.(19) and (20), taking into account relations (21) and (22). In order to see if it is fulfilled for higher frequencies, f_2 must be evaluated. This can be done by putting m=2 in eq.(11):

$$\frac{\partial}{\partial v}\left[v^2(D+H_o)\frac{\partial f_2}{\partial v} + v^2 F f_2\right] = -2i\,\omega\, v^2 f_2 - \frac{\partial}{\partial v}\left[v^2 H_1 \frac{\partial f_1}{\partial v}\right] \qquad (25)$$

Here terms of the order of $H_3\frac{\partial f_{-1}}{\partial v}$ have been neglected. This is justified by the fact that with a sine-modulated power $H_3=0$, while with a square-wave modulated power $H_3 << H_1$.

Eq.(25), once f_1 is known, can be solved with the same procedure described above, thus allowing for an extimation of f_2.

We have in this way shown that conditions (24) are fulfilled for all experimental scenarios considered in this paper (ie:

$\nu \geq 5$ Hz, P ~ 1 MW). In fact, for the whole energy range, even at the lowest frequency used, the ratio $H_1 \frac{\partial f_2}{\partial v}/\phi$ never exceeds 0.1 and it decreases rapidly with increasing frequency.

The accuracy at lower frequencies can be improved by inserting into eq.(13) the neglected term obtained from the solution of eq.(25). On the other hand, at low frequencies, we expect the particle transport to play such an important role as to violate the particle conservation condition.

For this reason, in the following, we shall restrict our analysis to frequencies higher than 5 Hz.

4. SIMULATION OF RESULTS IN THE STATIONARY CASE

The neutral hydrogen flux emanating from the plasma along the analyser line of sight per unit solid angle with energy between ε and $\varepsilon+d\varepsilon$ is given by

$$\Gamma(\varepsilon)\, d\varepsilon = \frac{d\varepsilon}{4\pi} \int_{x_1}^{x_2} n_H \left[n_o \langle \sigma_{cx}\, v \rangle + n_e \langle \sigma_R v \rangle \right] f(\varepsilon)\, \varepsilon^{1/2}\, \eta(\varepsilon,x)\, dx \qquad (26)$$

n_H, n_e and n_o being the minority ion, electron and neutral densities. The charge exchange $\langle \sigma_{cx} v \rangle$ and the recombination $\langle \sigma_R v \rangle$ reaction rates are averaged over the neutral and electron distribution functions respectively, so that $\langle \sigma_{cx} v \rangle$ depends on ε and, slightly, on the neutral temperature while $\langle \sigma_R v \rangle$ depends only on the electron temperature. The minority distribution function, assumed constant over a magnetic surface, is normalyzed so that $\int f(\varepsilon)\, \varepsilon^{1/2}\, d\varepsilon = 1$. The integration is performed along the line of sight and x_1 and x_2 are the coordinates of the intersection with the outermost plasma magnetic surface.

The probability $\eta(x,\varepsilon)$ for a neutral, generated at a location x with energy ε, to reach the plasma edge travelling along the line of sight is given by

$$\eta(x,\varepsilon) = \exp\left[- \int_x^{x_2} \frac{n_e \langle \sigma_{ie} v \rangle + \sum n_\alpha \langle \sigma_{cx}^\alpha v \rangle}{v}\, d\xi \right] \qquad (27)$$

where v is the neutral velocity, $\langle \sigma_{ie} v \rangle$ is the electron impact ionisation reaction rate. The summation is performed over all ion species in the plasma. The impurity contribution to the mean free path is taken into account by using the approximate relationship, $\langle \sigma_{cx}^\alpha v \rangle \simeq Z_\alpha \langle \sigma_{cx}^H v \rangle$ /18/, so that the summation is simply replaced by $n_e \langle \sigma_{cx}^H v \rangle$.

The ion and electron densities and temperatures are assumed to be constant over a magnetic surface. The shape of the magnetic surfaces is calculated by means of an MHD equilibrium code /19/.

In order to determine the neutral density profile to be used in eq.(26) we take advantage of the fact that each analyser measures also the energy spectra of the deuterium ions. The deuterium flux is obtained replacing in eq.(26) n_H with n_D and $f(\varepsilon)$ with a maxwellian distribution function. The neutral density profile is then computed by means of 1-D neutral transport code, similar to the one described in ref./20/, replacing the actual D-shaped magnetic surface cross-sections with circles of the same area.

The n_o profile obtained in this way is in good agreement with the poloidally averaged neutral density calculated by more sophisticated 3-D codes /21/. The dependence of n_o on the poloidal angle, which may be expected due to elongated plasma and, mainly, to inhomogenity of the neutral sources at the plasma edge are taken into account by using the edge neutral density as a free parameter thus assuming different values for different lines of sight.

These values, together with the ion temperature profiles, are adjusted in order to make the calculated deuterium fluxes reproduce the experimental ones. In fig.3 the computed deuterium fluxes are compared with the ones measured with the 4 analysers in operation at the time of the experiment.

The data refer to a JET discharge with $n_e = 2.7 \times 10^{19}$ m^{-3} and P_{RF}=3 MW. In fig.4 the electron temperature measured by electron cyclotron emission /22/ and the density from Far Infrared interferometer /23/ are shown together with the ion temperature profile obtained with the flux simulation /24/. In the calculation a value of 0.6 has been used for the ratio n_D/n_e.

This value is the one that gives consistency between the ion temperature profile obtained from NPA data and the measured neutron yield; it is nevertheless affected by an important uncertainty, which we estimate to be of about 30%.

In order to simulate the minority neutral flux we make use of the distribution function given by eq.(14), which depends on H_o which is fully determined by the parameter K, the RF induced diffusion coefficient in the limit $v \to 0$.

So, by using, in eq.(26), the neutral density and ion temperature profiles reproducing the neutral deuterium emission, the radial profile of K, represented by a suitable fitting expression, is adjusted as to make the calculated H fluxes reproduce the experimental ones. In the small Larmor radius limit ($k_\perp v_\perp / \omega_{ci} \to 0$) K is connected to the absorbed power density W, by /12/:

$$K = \frac{W}{3 n_H m_H} \qquad (28)$$

where n_H and m_H are the density and mass of the hydrogen ions respectively. In our case due to the low level of W eq.(28) still holds with good approximation. For this reason, in the following, we will always show the shape of W (ref. fig.7) as it has a more immediate physical meaning.

The results of this calculation are shown in fig.5, where the measured neutral hydrogen fluxes have been simulated for the same discharge considered above.

The hydrogen concentration in absence of RF can be obtained from the analysis of hydrogen and deuterium fluxes assuming both species have the same temperature.

In the ohmic phase of the discharge considered here a value constant over the plasma cross-section of $n_H/n_D = 0.05$ was obtained.

However, assuming a flat n_H/n_D profile also during the RF heated phase of the discharge, it has not been possible to simulate the hydrogen fluxes simultaneously on all lines of sight. To this end we had to assume that the hydrogen concentration increases inside the region of interaction. This can be explained, from the physical point of view, assuming that a strong distortion of the minority distribution function leads to important changes of its diffusion properties.

In fact if the diffusion coefficient D depends on the minor radius, the diffusive part of the particle flux is given by $J_H=\frac{\partial}{\partial r}(D\ n_H)$ /25/, where, following either a classical or neoclassical picture, the diffusion coefficient $D\propto \int \rho_L^2/\tau\ \ f\ d^3v$ is proportional to the inverse of the square root of the average energy. Making then the assumption that both the sources and the convective fluxes are not affected by the ICRF power one gets $D'n_H'=Dn_H$ that is

$$n_H' = \frac{D}{D'}\ n_H = n_H\ \frac{\int \rho_L^2/\tau\ \ f_{max}\ d^3v}{\int \rho_L^2/\tau\ \ f\ d^3v} \qquad (29)$$

where n_H' is the steady state H density during the RF pulse, f_{max} is the Maxwellian distribution function, f is the distribution function calculated by means of eq.(14) and n_H is the hydrogen density in the ohmic phase.

The radial profile of the n_H/n_D ratio calculated with eq.(29) and used to simulate the data of fig.5 is shown in fig.6.

At this point it is important to note that the global particle balance is not sensibly affected because the variation of the number of hydrogen ions in the interaction region is only a small fraction of the total number of hydrogen ions in the whole plasma.

In fig.7 the absorbed power profile computed with eq.(28) is shown together with the power transferred from the minority hydrogen ions to the background ions and to the electrons.

The total absorbed power results to be 1.3 MW of which 0.6 MW are going to the background ions and 0.7 MW to the electrons. In this case 3 MW of ICRF power were launched establishing the overall RF efficiency to 43%. The experimental measurements of the RF efficiency in JET is derived from the slope variation of the diamagnetic energy signal at the onset of the RF pulse. It gives a figure of ~ 80%. The discrepancy with the value obtained from the simulation is caused by the uncertainty of the deuterium dilution. This in return affects the value of the hydrogen density and finally generates large error bars on the total power density. Indeed, if the ratio n_D/n_e is varied within the range of its experimental error bars, the total power changes within a factor of 2. The total power deduced from this simulation is therefore globally in fair agreement with the experimental one.

More specifically, this indetermination affects mainly the fraction of power damped by electrons, while the one transferred to the background ions remains approximately constant (within 15%).

This is well understood taking into account the fact that the power is transferred to the electrons mainly through the high energy part of the distribution function which is partly out of the range of observation. However, an extension of the experimental energy range would not be very useful in the framework of the present model as the anisotropy of the distribution function increases with energy.

Finally, the peaking of the power deposition profile is clearly evidenced with an extension of .4 m at half maximum. This compares well with the results of the analysis of the rate of variation of T_e presented in ref./26/.

5. ANALYSIS OF MODULATED DISCHARGES

The behaviour of the distribution function is illustrated in fig.8, where the modulus and phase of the zeroth and first harmonic components are shown as calculated according to the formalism presented in section 3. For the sake of simplicity a sine wave modulation has been assumed for the quasi-linear diffusion coefficient: $H(v) = H_o(v)\ (1 + \sin \omega t)$ where $H_o(v)$ is given by eq.(4). $H_o(0) = K$ is connected to the stationary absorbed power level by eq.(28). The plasma parameters used in the calculation are: $n_e = 3 \times 10^{19}\ m^{-3}$, $n_D = 0.6\ n_e$, $n_H/n_D = 0.05$, $T_e = T_i = 4$ keV.

Some interesting features of the phase versus energy behaviour should be pointed out. First of all, at high energies the phase is close to $\pi/2$; this reflects the fact that in this energy range the tail dumping time is much longer than the modulation period. At low energies, on the other hand, the phase becomes less than zero. This is imposed by particles conservation: in fact the increase in the high energy population must be compensated by a corresponding decrease in the low energy one. The absorbed stationary power in this case was 0.128 MW/m^3 about 40% of which is deposited on the electrons and 60% on the ions. The amplitude of the oscillating absorbed power has the same value as the stationary one independently of the frequency and its phase-shift relative to the driving power is zero. This because, due to the relatively low power level, the finite Larmor radius effects do not play an important role and the power absorption does not depend on the instantaneous form of the distribution function but only on the amplitude of the wave electric field.

Since the power modulation experiments are mainly carried out to infer the stationary power deposition profile from the local oscillation of the electron and ion temperatures, it is of particular interest to analyse the oscillating part of the power delivered to electrons, $\hat{P}_e$, and to the ions, $\hat{P}_i$.

The frequency behaviour of amplitude and phase of $\hat{P}_e$ and $\hat{P}_i$, for the mentioned plasma parameters, is reported in fig.9, where the stationary powers deposited on the ions, P_{io}, and on the electrons, P_{eo}, are also indicated.

It is interesting at this stage to underline the following features: first of all, even if amplitude and phase of the total absorbed power do not depend on the frequency, $P_i(\nu)$ and $P_e(\nu)$ show a frequency dependence which, although weak in the considered range, makes $P_e(\nu)$ change by a factor of ~3 when the frequency is increased from 5 to 20 Hz. Moreover, in spite of the fact that the amplitude of the oscillating power is equal to the stationary one, $P_e(\nu)$ and $P_i(\nu)$ are much lower than P_{eo} and P_{io} respectively. This can be explained by considering that in this non-stationary situation power is required in order to continuously generate the fast ion tail. Finally, as it can be seen from fig.9, $P_i(\nu)$ and $P_e(\nu)$ are phase shifted with respect to the driving power. In the situation considered here this phase shift is close to $\pi/2$ for $\hat{P}_e$ while it is lower for $\hat{P}_i$.

It becomes evident at this point that the interpretation of data from modulation experiments requires some prudence. In fact, at least for the case considered here, the power deposition profile cannot be directly obtained from the measurements of temperature oscillations.

In order to compare the computed minority distribution function with the experimental data we remind that the measured neutral fluxes are connected to the distribution function through eq.(26), where other quantities like n_o, T_i etc are present. Following the procedure previously described, we get the profiles of those quantities from the analysis of deuterium fluxes. Once the neutral density and ion temperature are known the analysis of the stationary hydrogen fluxes can be carried out.

This is done by putting in eq.(26) the solution, for $f_o(v)$, obtained from the set of equations (16) to 20) and by adjusting the profile of K(r) until the agreement with the experimental data is reached, taking H_1/H_o=0.64 which is the correct value for a square wave modulation with zero lower level. In this way also the oscillating part of the distribution function is obtained.

It should be noted at this point that, in the range of parameter here considered, the modulation does not affect the stationary distribution function. In fact the solution obtained from eq.(14) is practically coincident with the one obtained solving the complete set of equations.

In fig.10 the calculated and experimental neutral hydrogen stationary fluxes are reported for a discharge with n_e = 3.4×10^{19} m^{-3}, T_e = 3.6 keV, T_i = 3.3 keV, heated with a peak RF power of 1.5 MW (0.75 MW stationary level) square wave modulated at a frequency of 12.5 Hz. In fig.11 the stationary absorbed power density profile is shown together with the power density to the ion and electron bulk. In this case most power is absorbed by the ions (70%). This is what can be expected because, due to the low power level, the high energy part of the distribution function, which gives its energy mainly to the electrons, is not strongly developed. For the same reason the increase of the ratio n_H/n_D in the deposition region is quite moderate.

At this point the oscillating part of the hydrogen distribution function calculated as described at each plasma position can be inserted in eq.(26) to calculate the oscillating part of the neutral fluxes, $\hat{\Gamma}_1$, which can be directly compared with the experimental data obtained with the analysis described in section 1.

Such a comparison is shown in fig.12, where the energy behaviour of the phase of $\hat{\Gamma}_1$ and of the ratio $|\Gamma_1|/\Gamma_o$ as calculated with the described analysis are reported together with the experimental values for the same considered shot.

The agreement is quite satisfactory mainly if the fact that no adjustable parameters are used in this calculation is taken into account, all needed information being obtained by the stationary analysis.

The same comparison is reported in fig.13 for a similar discharge modulated with a frequency of 5 Hz.

6. SUMMARY AND CONCLUSIONS

We have shown in the previous sections a simulation and a comparison with the experimental results of the fluxes of neutral atoms, deuterium and hydrogen, emitted by a JET plasma heated with both a stationary and a modulated level of ICRF power in the hydrogen minority scheme.

The distribution function of the deuterium ions, showing no tail, has been assumed maxwellian.

To compute the distribution function of the minority ions we have used a one dimensional Fokker-Planck equation where the wave-particles interaction is described by a quasi- linear diffusion term in the velocity space. The effects of finite Larmor radius have been taken into account by assuming that the launched spectrum has only one component in $k_{\perp}$. By using the relevant plasma profiles which allow us to reproduce the deuterium fluxes and by shaping the profile of the quasi-linear diffusion coefficient we have been able to reproduce the hydrogen minority neutral fluxes measured by four analysers with different lines of sight. To do so we have had to assume that the minority concentration increases in the region of interaction which is close to the plasma centre. This has been ascribed to the variation of the diffusion properties of the resonating ions caused by the strong distortion of their distribution function.

The overall result is that a large fraction of the total power is absorbed by the minority near the plasma centre.

The determination of the total absorbed power is affected by a large error due both to the uncertainties in the knowledge of some plasma quantities (eg the ion density) and to the fact that only part of the spectrum is measured ($E<100$ KeV). An extension of the measured energy range would not be very useful in the frame of the present model as the anisotropy of the distribution function becomes more important when the energy is increased. Nevertheless the part of the RF power

which is eventually dumped on the ion population can be determined quite accurately with the present model.

In order to simulate the neutral fluxes during the modulated discharges we have expanded the Fokker-Planck equation in Fourier components. The resulting set of ordinary differential equations has been solved with the boundary conditions imposed by particles conservation providing both the stationary and the oscillating (real and imaginary) part of the minority distribution function. The hydrogen fluxes thus computed are in good agreement with the measured ones.

This means that the acceleration of the resonating ions is well described by the quasi-linear diffusion term while the Coulomb collisions are responsible for the dumping of the ion tail with the consequent heating of the plasma bulk.

Finally, we have demonstrated that the expansion of the Fokker-Planck equation in Fourier components gives a sensible result in terms of the perturbed distribution functions at frequencies larger than a few hertz. This is of considerable interest for further analysis of power balance during modulation experiments in the minority heating scheme.

ACKNOWLEDGEMENTS

The authors would like to acknowledge the great effort produced by the RF Division in putting up the experiment, as well as the one of the various operational teams in running the machine. Particular thanks to W Core, F De Marco, W Engelhardt, C F F Karney and S E Segre for very useful discussions.

REFERENCES

/1/ HOSEA J, BERNABEI S, COLESTOCK P, DAVIS S L, EFTHIMION P, et al., Phys. Review Lett. 43 (1979) 1802

/2/ MIURA Y, MATSUMOTO H, KIMURA H, ODAJIMA K, MORI M et al., Nuclear Fusion 24 (1984) 211

/3/ TFR Group, Nuclear Fusion 25, (1985) 1719

/4/ REBUT P H, BARTLETT D V, BÄUMEL G, BEHRINGER K, BEHRISCH R et al., Proc. 10th Int. Conf. on Plasma Phys. and Controlled Nuclear Fusion Research, IAEA-CN-44/A-I-1, London, 1984

/5/ BICKERTON R J, ALLADIO F, BARTLETT D V, BEHRINGER K, BEHRISCH R et al., Plasma Physics and Controlled Fusion, 28, 1A (1986) 55 - Invited paper at the 11th Europ. Conf. on Controlled Fusion and Plasma Physics, Budapest (1985)

/6/ JACQUINOT J, ANDERSON R, ARBEZ J, BARTLETT D, BEAUMONT B, et al., 'Preliminary ICRF results from JET', JET Report JET-P/85)09 - Invited paper at the Inst. of Physics Conference, Glasgow (1985)

/7/ JACQUINOT J, ANDERSON R, ARBEZ J, BARTLETT D, BEAUMONT B et al., Plasma Physics and Controlled Fusion, 28, 1A (1986) 1 - Invited paper at the 12th Europ. Conf. on Controlled Fusion and Plasma Phys., Budapest (1985)

/8/ BHATNAGAR V P, BARBATO E, BOSIA G, EVRARD M P, GAMBIER D et al., Proc. of the 13th Eurp. Conf. on Controlled Fusion and Plasma Heating, vol.II, 193, Schliersee (1986)

/9/ BARBATO E, GIANNELLA R, Physics Letters, 110A (1985) 309

/10/ BARTIROMO R, BRACCO G, BRUSATI M, GROSSO G, MANTOVANI S, TILIA B, ZANZA V, Rev. Sci. Instr. 58 (1987) 788

/11/ BRIGHAM E O, 'The Fast Fourier Transform' Prentice Hall, Engelwood Cliffs (1974)

/12/ STIX T H, Nuclear Fusion 15 (1975) 737

/13/ ANDERSON D, ERIKSSON L G, LISAK M, Nuclear Fusion 25 (1985) 1751

/14/ GAMBIER D J, SAMAIN A, Nuclear Fusion 25 (1985) 283

/15/ TRUBNIKOV B A in 'Reviews of Plasma Physics', ed. M A Leontovich, Consultants Bureau NY (1985), vol.1, 105

/16/ KARNEY C F F, Computer Physics Reports, vol.4, no.3/4 (1986) 183

/17/ NAG Fortran Lybrary Manual - Mark 11, Numerical Algorithms Group, Oxford (UK) and Downers Grove, Illinois (1984), vol.1, D02

/18/ GILBODY H B, Physica Scripta 24 (1981) 712

/19/ BRUSATI M, CHRISTIANSEN J P, CORDEY J G, JARRET K, LAZZARO E, ROSS R T, Computer Physics Reports, vol.1, no.7/8 (1984) 345

/20/ TAMOR S, Journal of Comput. Physics. 40 (1981) 104

/21/ SIMONINI R, TARONI A, Proc. of the 13th Europ. Conf. on Controlled Fusion and Plasma Heating, vol.I, 164, Schliersee (1986)

/22/ COSTLEY A E, BAKER E A M, BRUSATI M, BARTLETT D V, CAMBELL D J et al., Proc. of the 12th Europ. Conf. on Controlled Fusion and Plasma Physics, vol.I, 227, Budapest (1985)

/23/ BRAITHWAITE G, BULLIARD A, BRUNEAU J L, HANCOCK J, MAGYAR G et al., 'The Multichannel Far Infrared Interferometer (KG1) on JET', JET Report JET-IR(85)08-(1985)

/24/ CORTI S, BARBATO E, BRACCO G, BRUSATI M, BURES M et al., Proc. of the 13th Europ. Conf. on Controlled Fusion and Plasma Heating, vol.I, 109, Schliersee (1986)

/25/ BRAGINSKII S I, in 'Reviews of Plasma Physics' ed. M A Leontovich, Consultants Bureau N.Y.(1965), vol.1, 205

/26/ JACQUINOT J, ANDERSON R J, ARBEZ J, BARTLETT D, BEAUMONT B et al., Plasma Physics and Controlled Fusion 28, 1A (1986) 1

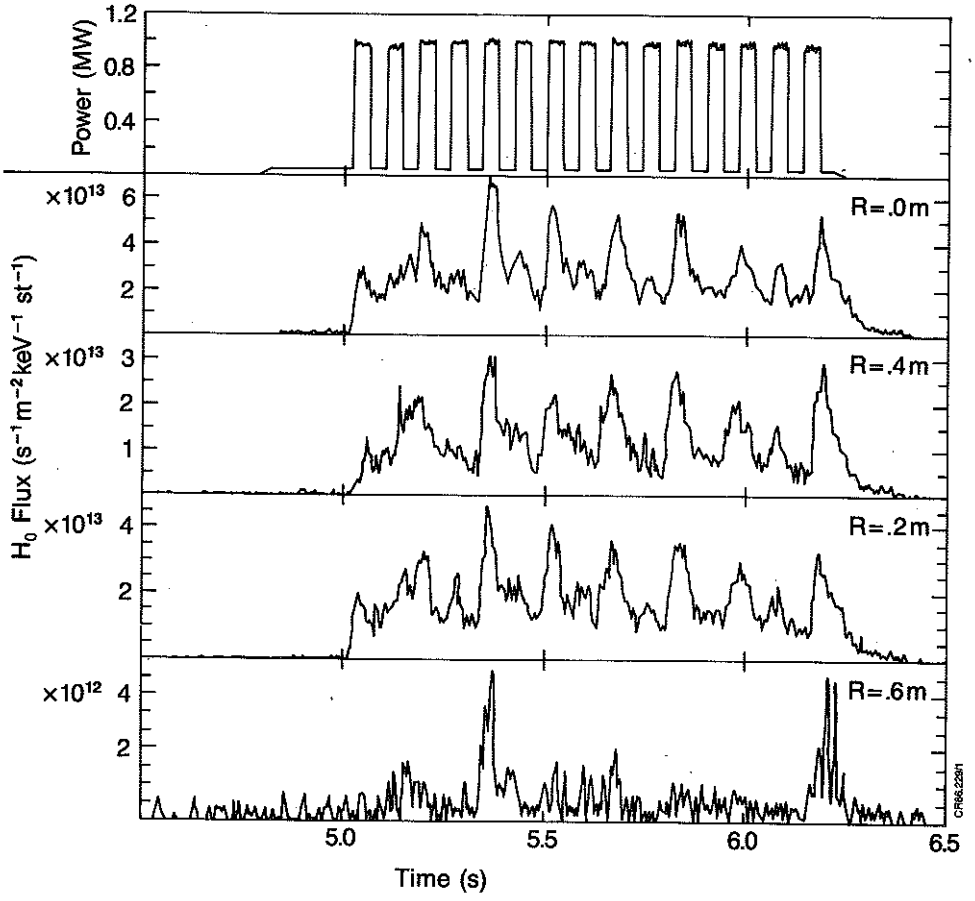

Fig.1 Total modulated RF coupled power and neutral hydrogen fluxes at 40 keV as measured by four analysers with lines of sight crossing the plasma at different radii (R).

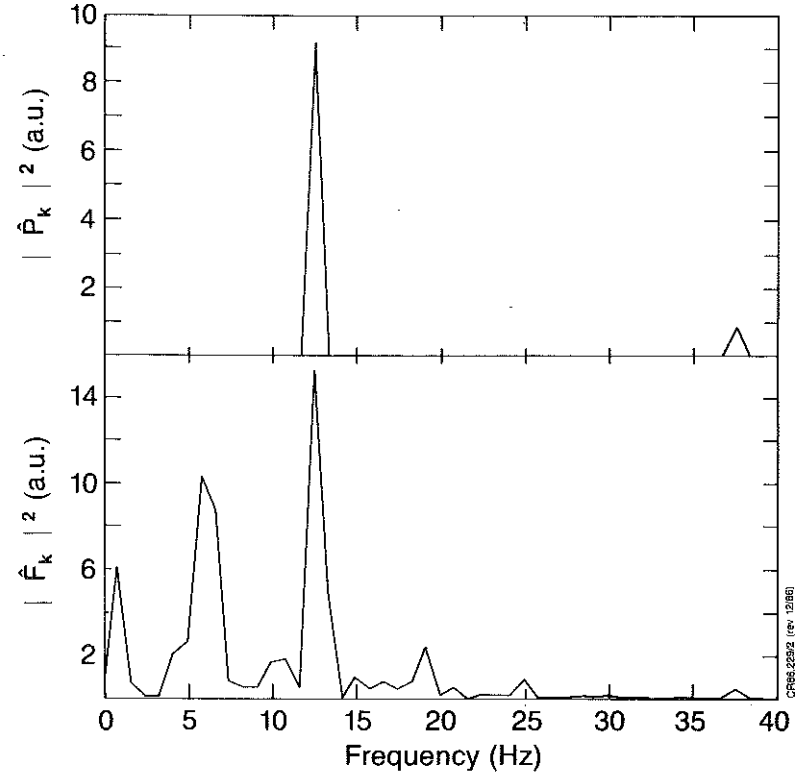

Fig.2 Autocorrelation spectra of power (a) and neutral flux (b). The side peak at about 6 Hz corresponds to the sawtooth oscillations.

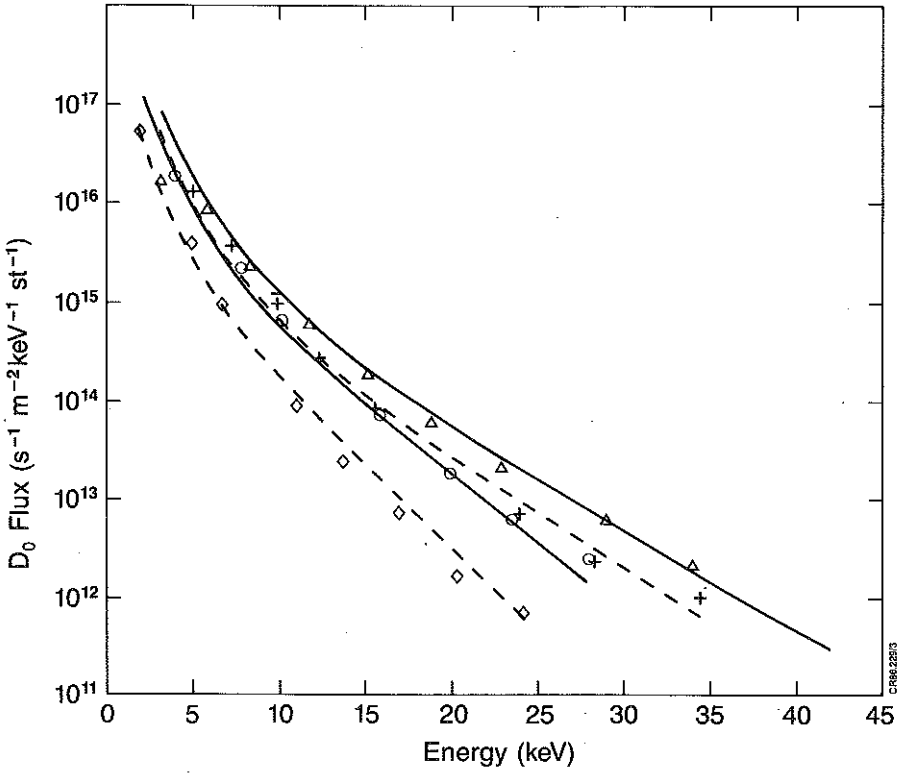

Fig.3 Comparison of computed deuterium fluxes (lines) with measured ones for four different analysers [(Δ) R=0; (+) R=.2; (o) R=.4 and (◇) R=.6 m].

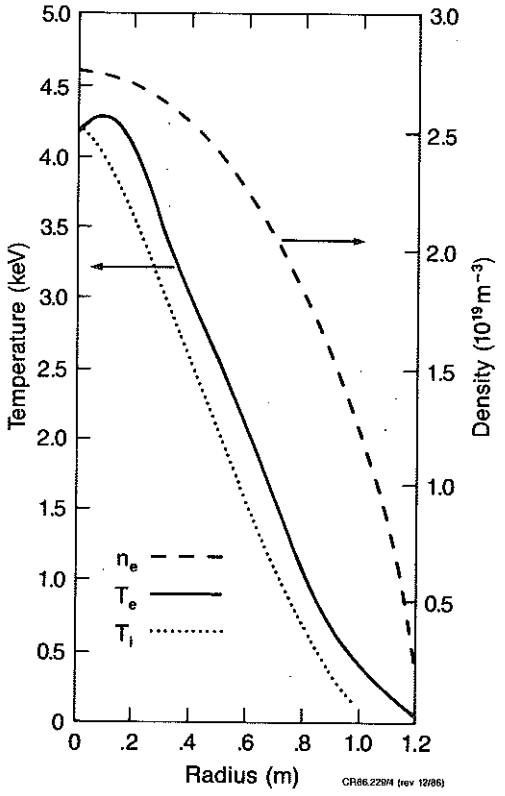

Fig.4 Experimental profiles of T_e (from ECE), n_e (from FIR interferometer) and T_i (from flux simulation).

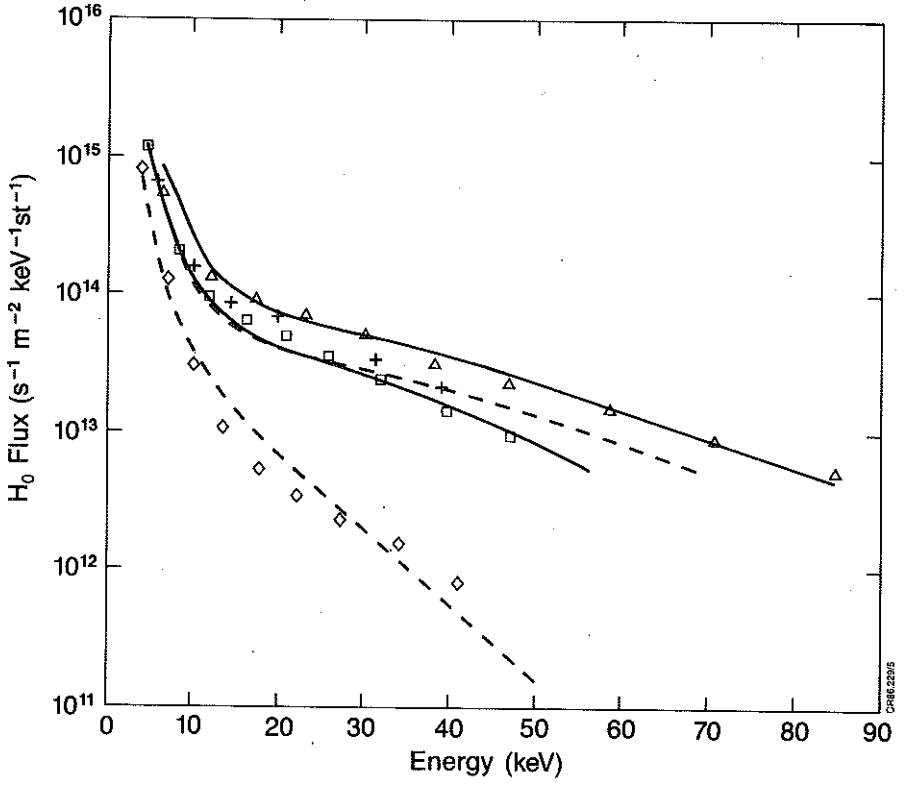

Fig.5 Comparison of computed hydrogen fluxes (lines with measured ones [(Δ) R=0; (+) R=.2; (□) R=.4 and (◇) R=.6 m].

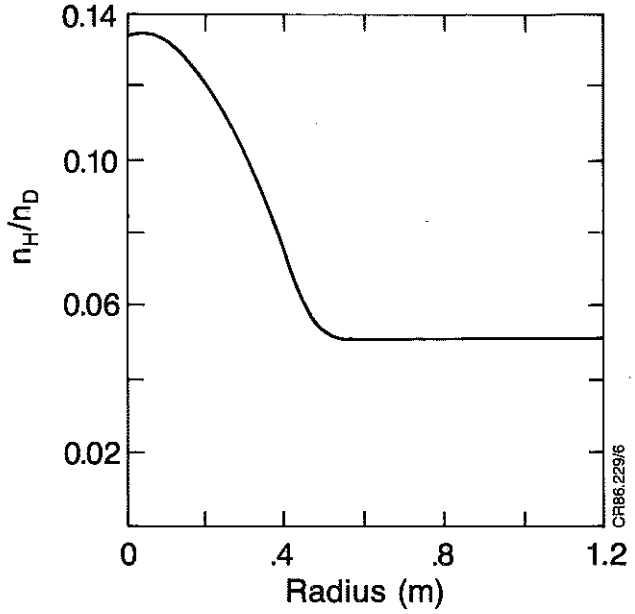

Fig.6 n_H/n_D ratio vs. radius assumed for the simultaneous fit of the H spectra.

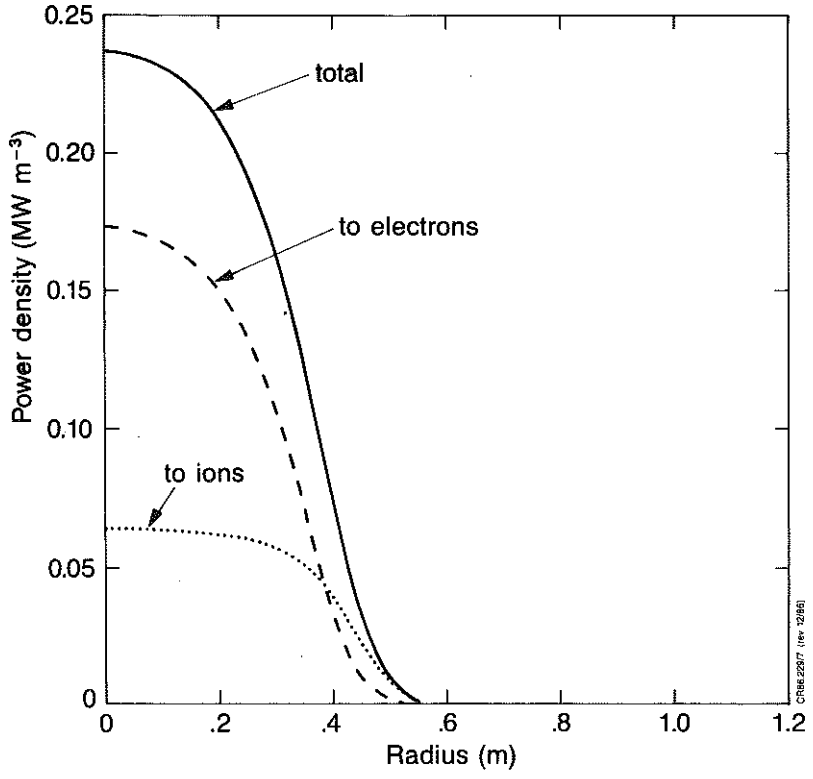

Fig.7 Profiles of total absorbed power density and of fractions delivered to electrons and ions.

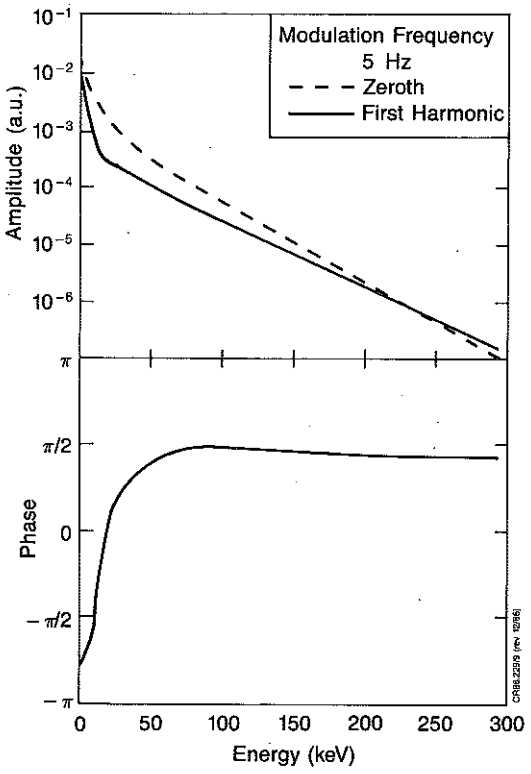

Fig.8 Amplitude and phase of zeroth and first harmonic components for f_{mod}=5 Hz.

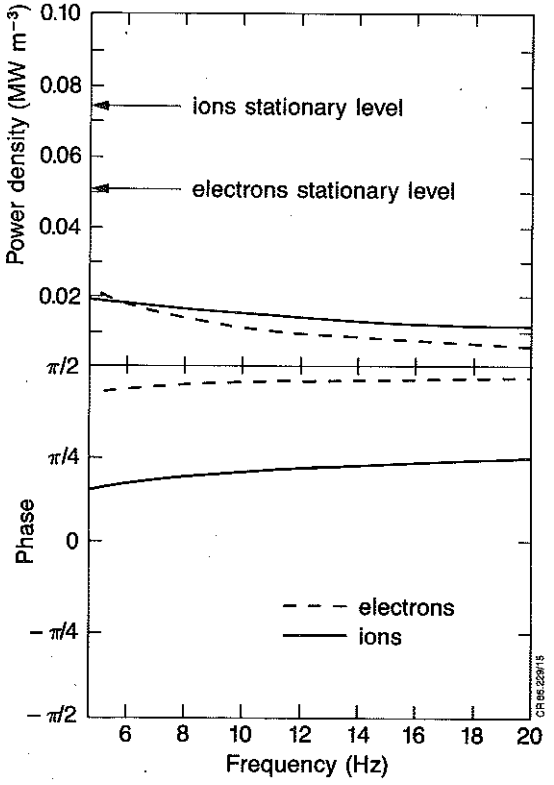

Fig.9 Modulation frequency behaviour of amplitude and phase of first harmonic of power going to ions and electrons. The two arrows show the stationary levels.

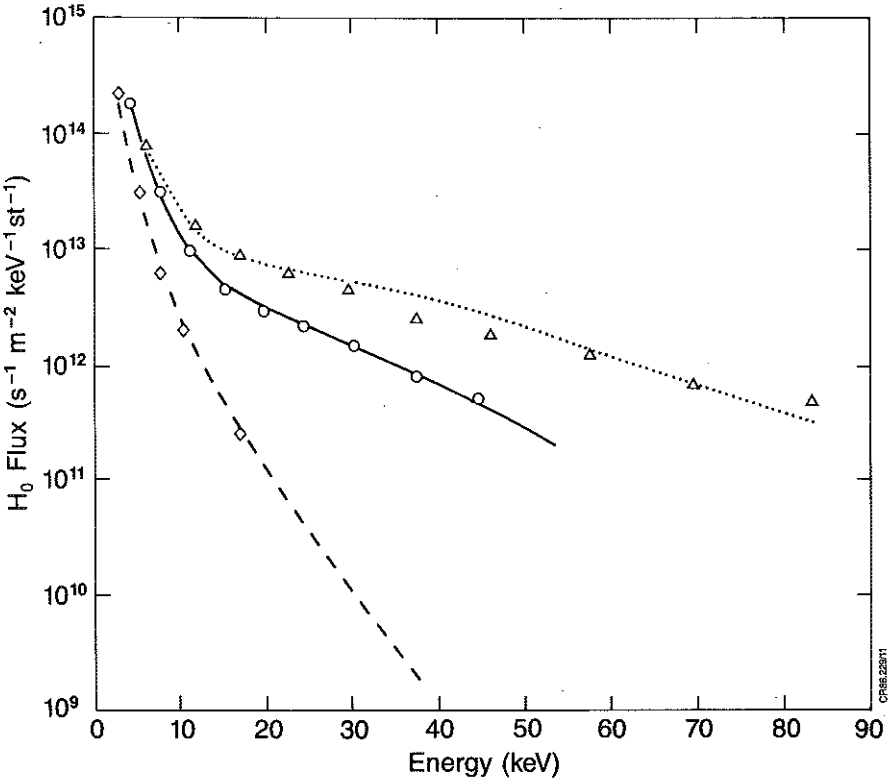

Fig.10 Comparison of computed hydrogen stationary fluxes with measured ones [(Δ) R=0; (o) R=.2 and (◇) R=.6 m].

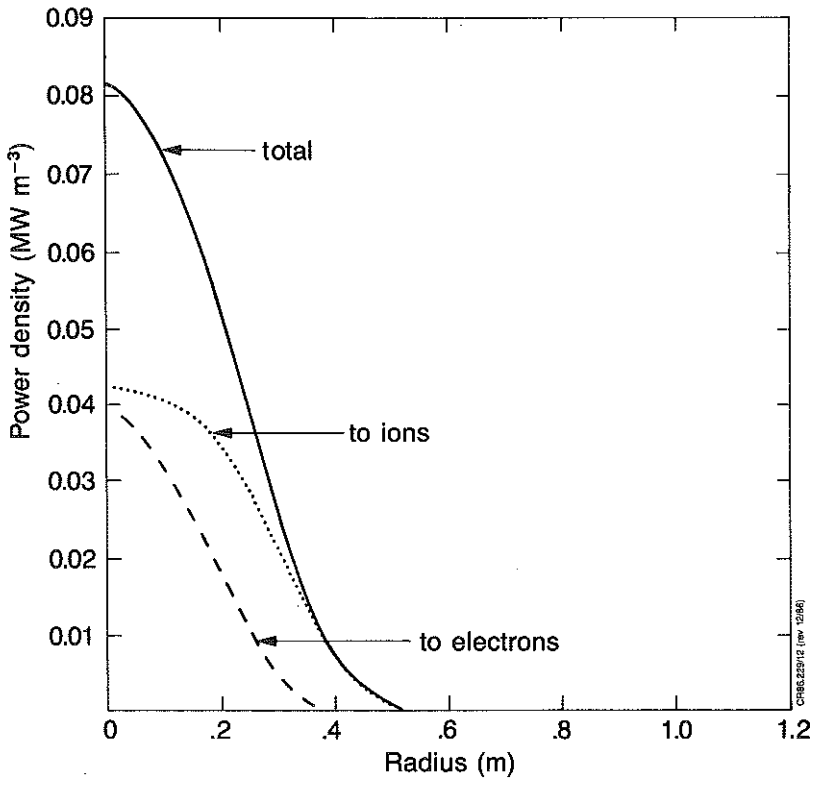

Fig.11 Profiles of total stationary absorbed power density and of fractions deposited on ions and electrons.

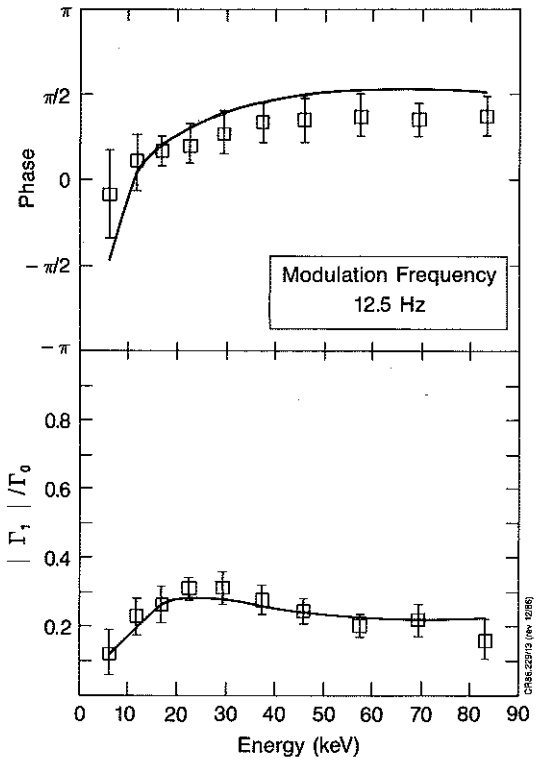

Fig.12 Comparison of computed energy behaviour of $\hat{\Gamma}_1$ phase and of $|\Gamma_1|/\Gamma_0$ with experimental values [f_{mod}=12.5 Hz].

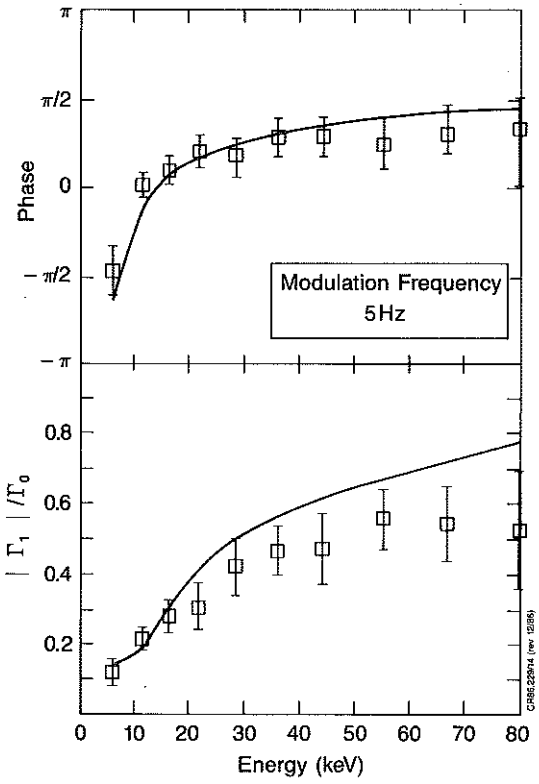

Fig.13 Same as Fig.12, with f_{mod}=5 Hz.